Forced Cenozoic continental subduction of Tarim craton-like lithosphere below the Tianshan revealed by ambient noise tomography

Weijia Sun[1*], Songjian Ao[2*], Qingya Tang[1], M. G. Malusà[3*], Liang Zhao[2] and Wenjiao Xiao[4,2]

[1] Key Laboratory of Earth and Planetary Physics, Institute of Geology and Geophysics, Chinese Academy of Sciences, Beijing 100029, China.

[2] State Key Laboratory of Lithospheric Evolution, Institute of Geology and Geophysics, Chinese Academy of Sciences, Beijing 100029, China.

[3]Department of Earth and Environmental Sciences, Department of Earth and Environmental Sciences, University of Milano-Bicocca, 20126 Milan, Italy.

[4] Xinjiang Research Center for Mineral Resources, Xinjiang Institute of Ecology and Geography, Chinese Academy of Sciences, Urumqi 830011, China.

**Correspond to WS: swj@mail.iggcas.ac.cn; SA: asj@mail.iggcas.ac.cn; MM: marco.malusa@unimib.it*

ABSTRACT

The possibility that craton-like lithosphere may undergo subduction during convergence of major tectonic plates is still poorly investigated. Here we tackle this issue by ambient noise tomography of the Tarim Basin and the Tianshan. Our S-wave velocity model reveals a flat-lying high-velocity anomaly beneath the Tarim Basin in the 45-60 km depth range, consistent with intrusion of mafic rocks at the base of the lower crust above a depleted lithospheric mantle, as expected after interaction of the lithosphere with a mantle plume. This high-velocity anomaly

can be followed northward, steeply dipping (~45°) beneath the Tianshan, which indicates that the Tarim craton-like lithosphere was subducted to mantle depths. It is connected with a fast P-wavespeed anomaly in the upper mantle, interpreted as a relict of the South Tianshan Ocean. A long period of tectonic quiescence, after the closure of the South Tianshan Ocean and before the Cenozoic tectonic rejuvenation of the Tianshan, suggests a minor role of oceanic slab pull in controlling continental subduction. The major player is instead the northward push of India within the framework of Cenozoic India-Asia convergence. We conclude that forced subduction can be experienced not only by thinned continental crust but also by a strong craton-like lithosphere.

INTRODUCTION

Continental subduction has long been considered impossible due to the intrinsic positive buoyancy of the continental crust (McKenzie, 1969), but is now widely documented by petrological and geophysical evidence (Guillot et al. 2009; Kufner et al., 2016; Malusà et al., 2021), even in the absence of a precursor oceanic slab providing the driving force by negative buoyancy (Sun et al., 2019). However, the possibility that craton lithosphere may undergo forced subduction during convergence of major tectonic plates is still poorly investigated. The Tarim Basin in Central Asia (Fig. 1A) is a favorable site to tackle this issue. It is floored by a strong craton-like lithosphere, and it is in a key position within the framework of Cenozoic India-Asia collision. However, unlike the nearby Pamir and Hindu Kush (Kufner et al., 2016; Bloch et al., 2021), its deep tectonic structure is not sufficiently constrained by high-resolution geophysical data. Here we employ ambient noise tomography to study the lithospheric structure of the Tarim and nearby regions. Our results demonstrate that forced continental subduction can be

experienced not only by thinned continental crust, but also by a strong craton-like lithosphere in areas of strong convergence between major tectonic plates.

GEOLOGIC BACKGROUND

The Tarim Basin is located in northwestern China between the Tibetan Plateau to the south, the Pamir to the west, and the Tianshan to the north (Fig. 1A). Its Precambrian basement consists of continental blocks that amalgamated during the Neoproterozoic (Guo et al., 2005; Yang et al., 2018). Cenozoic strata are largely undeformed (Jia, 1997). Two major events affected the Tarim basement during the Phanerozoic: an early Paleozoic reactivation of the Neoproterozoic suture zone and a widespread Early Permian (300–270 Ma) igneous activity forming a large igneous province (LIP in Fig. 1A) possibly induced by a mantle plume (Xu et al., 2014). Based on high-resolution aeromagnetic data, it has been recently suggested that plume-lithosphere interactions may have strengthened the Tarim lithosphere with the formation of a strong mantle keel and the intrusion of mafic rocks into the lower crust (Xu et al., 2021). However, seismic tomography evidence supporting this interpretation is still lacking.

To the north of the Tarim Basin, the Tianshan stretches from E to W for more than 2000 km (Fig. 1A). The tectonic framework of this multi-phased orogenic belt was established in the Late Carboniferous (Gao et al., 2008) or the Late Permian-Triassic (Abuduxun et al., 2021; Xiao et al., 2013) and reactivated during the Cenozoic in response to India–Asia collision (Abdrakhmatov et al., 1996; Shu et al., 2003; Li et al., 2022). The first significant evolution stage of the Tianshan involved arc accretion, oceanic subduction, and continental collision (Han et al., 2011; Xiao et al., 2015). Ultrahigh pressure rocks derived from mid-ocean-ridge basalts attest to oceanic subduction and subsequent exhumation of deeply buried rocks in the Late Carboniferous (Gao et al., 2008) or the Late Triassic. Zircon U–Pb ages as young as 224-217 Ma (Sang et al.,

2016) likely mark the final closure of the South Tianshan Ocean, a branch of the Paleo-Asian Ocean, and the consequent collision between the Tarim lithosphere and the Yili-Kazakhstan shield (Han et al., 2011; Xiao et al., 2013) (Fig. 1A). The polarity of oceanic subduction is still controversial. Some studies suggest northwest-dipping subduction of the South Tianshan Ocean beneath the Yili-Kazakhstan shield (Abuduxun et al., 2021; Gao et al., 2008), whereas other studies either suggest southeast-dipping subduction beneath the Tarim Craton (Charvet et al., 2011; Wang et al., 2017) or bi-directional subduction (Ge et al., 2014; Wang et al., 2016). The existence of a subducted slab down to 400 km depth beneath the Tianshan is confirmed by teleseismic tomography (Koulakov, 2011), but the linkage with the uppermost mantle and crustal structures is still unclear. Cenozoic crustal shortening as large as 200-300 km (Avouac et al., 1993; Molnar and Tapponnier, 1975) may suggest a major stage of continental subduction after the closure of the South Tianshan Ocean. However, the possibility that continental crust rocks have reached mantle depths is still not demonstrated by tomography evidence.

METHODS

We collected the continuous waveforms recorded by 48 permanent broadband stations from Data Management Centre of China National Seismic Network (doi:10.11998/SeisDmc/SN), from October 2018 to October 2019, to image the crustal and uppermost mantle velocity structure of the Tarim lithosphere and surroundings using ambient noise tomography. The seismic stations (Fig. 1B) are distributed with an average interval of 100-200 km around the Tarim Basin. This ensures good coverage of the study area with seismic ray paths (Fig. 1B). We employed a frequency-domain approach to extract phase velocity dispersions from ambient noise (Hawkins & Sambridge, 2019) and invert the 3-D shear-wave velocity structure (Yoshizawa and Ekström, 2010). More details on the methods and tests are provided in Sections S1 and S2.

Robustness of the results and interpretations are extensively tested in Sections S3 and S4, similar to Cai et al. (2018).

RESULTS AND INTERPRETATION

Figure 2 shows representative sections of the inverted 3-D shear wave velocity model. Based on the resolution tests of Fig. S4, the model has a spatial resolution as high as 1.0°×1.0°. The vertical section from the northern edge of the Tibetan Plateau to Lake Issyk-Kul in Kyrgyzstan (Fig. 2A-C) reveals an increase in S-wave velocities beneath the Tarim Basin reaching as high as 4.2-4.3 km/s at 40-45 km depth (anomaly HV1 in Fig. 2B). Such S-wave velocities, which are also found above the Moho independently inferred from receiver function (He et al., 2014), are consistent with the presence of amphibolite (e.g., Malusà et al., 2021 their Fig. 4). This suggests a strengthened lithosphere due to intrusion of mafic rocks at the base of the lower crust. Starting from ~60-65 km depth, S-wave velocities decrease to ~4.0 km/s (Fig. 2B, F). The low-velocity anomaly found at depth > 70 km (LV3 in Fig. 2C) is consistent with a mid-lithosphere discontinuity recognized in many cratons, which reflects their evolution from craton formation to the present (Sun et al., 2020). The highest shear wave velocities in our model are found beneath Bachu (Fig. 2B), i.e., the proposed center of the Permian plume head based on analysis of high-resolution aeromagnetic data. Overall, the shear wave velocity structure beneath the Tarim Basin demonstrates a strengthened lower crust and a disturbed lithospheric mantle as expected after plume-craton lithosphere interaction (Xu et al., 2021).

The layered velocity structure beneath the Tarim Basin provides a suitable marker to reveal later stages of continental subduction. The flat-lying high-velocity anomaly HV1 can be followed farther north beneath the Tianshan (Fig. 2B), where it dips northwestward with an angle of ~45°. This steeply dipping anomaly provides clear indication that the Tarim lithosphere was

subducted to mantle depths beneath the Tianshan. Figure 2C shows the relative velocities in the 0-100 km depth range for easier comparison with the teleseismic tomography model of Koulakov (2011) in the 100-600 km depth range (Fig. 2D). The high-velocity anomaly HV1 revealed by ambient noise tomography is clearly connected with the P-wave high-velocity anomaly HV2 revealed by teleseismic tomography down to ~600 km depth, which is interpreted as a lithospheric slab dipping at an angle of ~70°. However, the S-wave velocity anomaly HV1 is much stronger than the P-wave velocity perturbation HV2 (5-6% vs 1.0-1.5%).

Above anomaly HV1, shear wave velocities reach as low as ~3.8 km/s at 50-70 km depth (LV1 in Fig. 2B). These values are consistent with both high-pressure quartzo-feldspathic gneisses and serpentinite (Malusà et al., 2021), and may either mark continental crust rocks involved within a subduction channel or a serpentinized mantle wedge due to activity of slab-released fluids. In Fig. 2C, the low-velocity anomaly LV1 can be traced down to ~90 km depth. In Fig. 2D, a P-wave low-velocity anomaly (LV2) is observed down to ~400 km depth. Both velocity perturbations LV1 and LV2 are consistently around 1% or smaller. Similar high- and low-velocity anomalies are also observed along a cross-section from the Tibetan Plateau to the Junggar Basin (Supplementary Fig. S1).

DISCUSSION AND CONCLUSIONS

Polarity of South Tianshan oceanic subduction

The tip of the steeply dipping high-velocity anomaly HV2 imaged by teleseismic P-wave tomography beneath the Tianshan (Koulakov, 2011) is interpreted as a relict of the South Tianshan Ocean. As anomaly HV2 is clearly connected with a high-velocity anomaly in the Tarim lithosphere revealed by ambient noise tomography, our findings provide clear evidence of north-dipping subduction of the South Tianshan Ocean beneath the Yili-Kazakhstan shield

during the Paleozoic-early Mesozoic (Abuduxun et al., 2021; Gao et al., 2008) (Fig. 3). Therefore, hypotheses of south-dipping or bi-directional subductions can be excluded. The low-velocity region in the mantle wedge atop the subducting slab attests to a major impact of slab fluids released during the oceanic subduction stage in the Paleozoic-early Mesozoic.

Subduction of Tarim lithosphere to mantle depths

Our 3-D shear wave velocity model across the Tarim Basin supports the hypothesis that mantle plume processes may have strengthened the Tarim lithosphere during the Permian (Xu et al., 2021), forming a stable craton-like continent after intrusion of mafic rocks at the base of the lower crust. The plume-head center was located near the present-day southern deformation front of the Tianshan (Fig. 3). The flat-lying high-velocity anomaly interpreted as Tarim mafic lower crust dips under the Tianshan at an angle of ~45°, providing clear indication of subduction of craton-like lithosphere to mantle depths, consistent with previous estimates of Cenozoic shortening. The cratonic lithosphere beneath the Tarim Basin efficiently transmitted the deformation associated to Cenozoic India-Asia collision northward across the Tianshan, where the lithosphere is weaker and not affected by plume activity. Geodetic GPS measurements show a northward decrease in crustal shortening rate from ~36 mm/yr in the Indian Plate to ~20 mm/yr on the southern front of the Tianshan (Gan et al., 2007; Zubovich et al., 2010; Fig. 1A). We conclude the remaining ~16 mm/yr is likely accommodated by active continental subduction of the Tarim lithosphere beneath the Tianshan.

Tarim lithosphere is subducted northwestward beneath the Tianshan in the east, whereas an arcuate slab of Asian lithosphere is subducted southeastward beneath the Pamir in the west (Pamir slab in Fig. 3). An even more complicated structure is documented in front of the Indian indenter beneath the Hindu Kush (Kufner et al. 2016), where Indian thinned lithosphere

subducted beneath Asia is torn off, forming a prominent high-velocity anomaly down to the mantle transition zone (Fig. 3). A similar behavior of opposite-dipping continental slabs is also documented under the European Alps, where the European continental lithosphere is subducted beneath Adria in the Western Alps, and the Adriatic continental lithosphere is subducted beneath the remnants of the Alpine subduction wedge in the Eastern Alps (Sun et al., 2019; Malusà et al., 2021). However, unlike Central Asia, no craton-like lithosphere was involved in the subduction below the Alps.

Mechanism of Tarim continental subduction

Slab pull generated by subducting oceanic lithosphere is generally considered as the major trigger for the onset of continental subduction (Davies, 1999). However, a very long period of tectonic quiescence (>150 Ma) characterized the study region after oceanic subduction and the closure of the South Tianshan Ocean. The Tianshan orogen was tectonically reactivated only in the Cenozoic in response to India–Asia collision (e.g., Li et al., 2022). Within this framework, and despite the evident connection at a depth between the South Tianshan oceanic slab and the Tarim continental lithosphere (Fig. 3), oceanic slab pull can be safely ruled out as a potential major player in controlling continental subduction of the Tarim lithosphere. Our results suggest that plate convergence and the northward push of cratonic India play a primary role in determining subduction of craton-like lithosphere beneath the Tianshan (Fig. 3), which was likely coeval with continental subduction beneath Hindu Kush and Pamir (Kufner et al. 2016; Bloch et al. 2021). Forced subduction of craton-like lithosphere was likely favored by the presence of inherited South Tianshan oceanic lithosphere already subducted to the north beneath the Tianshan. We conclude that forced subduction can be experienced not only by thinned continental crust sections, as documented in the European Alps (Sun et al., 2019), but also by a

strong craton-like lithosphere. Our results provide new insights on the dynamics of continental subduction and may find application to other areas characterized by fast and strong convergence between major tectonic plates.

ACKNOWLEDGMENTS

The constructive suggestions from three anonymous reviewers are thanked. This research is supported by National Natural Science Foundation of China (41888101, 42022026, 41822204, and 41774060). The S-wave velocity model can be accessed at Zenodo (https://doi.org/10.5281/zenodo.6901979).

REFERENCES CITED

Abdrakhmatov, K. Y., Aldazhanov, S. A., Hager, B. H., Hamburger, M. W., Herring, T. A., Kalabaev, K. B., et al. (1996). Relatively recent construction of the Tien Shan inferred from GPS measurements of present-day crustal deformation rates. Nature, 384(6608), 450-453. https://doi.org/10.1038/384450a0

Abuduxun, N., Xiao, W., Windley, B. F., Chen, Y., Huang, P., Sang, M., et al. (2021). Terminal Suturing Between the Tarim Craton and the Yili-Central Tianshan Arc: Insights From Mélange-Ocean Plate Stratigraphy, Detrital Zircon Ages, and Provenance of the South Tianshan Accretionary Complex. Tectonics, 40(7), e2021TC006705.

Avouac, J. P., Tapponnier, P., Bai, M., You, H., & Wang, G. (1993). Active thrusting and folding along the northern Tien Shan and Late Cenozoic rotation of the Tarim relative to Dzungaria and Kazakhstan. Journal of Geophysical Research: Solid Earth, 98(B4), 6755-6804. https://agupubs.onlinelibrary.wiley.com/doi/abs/10.1029/92JB01963

205 Bloch, W., Schurr, B., Yuan, X., Ratschbacher, L., Reuter, S., Kufner, S. K., et al. (2021).
206 Structure and stress field of the lithosphere between Pamir and Tarim. Geophysical
207 Research Letters, 48(22), e2021GL095413.
208 Cai, C., Wiens, D. A., Shen, W., and Eimer, M., 2018, Water input into the Mariana subduction
209 zone estimated from ocean-bottom seismic data: Nature, 563, 389-392.
210 Charvet, J., Shu, L., Laurent-Charvet, S., Wang, B., Faure, M., Cluzel, D., et al. (2011).
211 Palaeozoic tectonic evolution of the Tianshan belt, NW China. Science China Earth
212 Sciences, 54(2), 166-184. https://doi.org/10.1007/s11430-010-4138-1
213 Davies, G.F. (1999). Dynamic Earth. Cambridge University Press, New York.
214 Gan, W., Zhang, P., Shen, Z.-K., Niu, Z., Wang, M., Wan, Y., et al. (2007). Present-day crustal
215 motion within the Tibetan Plateau inferred from GPS measurements. Journal of
216 Geophysical Research, 112(B8).
217 Gao, J., Long, L., Klemd, R., Qian, Q., Liu, D., Xiong, X., et al. (2008). Tectonic evolution of
218 the South Tianshan orogen and adjacent regions, NW China: geochemical and age
219 constraints of granitoid rocks. International Journal of Earth Sciences, 98(6), 1221.
220 journal article. https://doi.org/10.1007/s00531-008-0370-8
221 Ge, R., Zhu, W., Wilde, S. A., He, J., Cui, X., Wang, X., & Bihai, Z. (2014). Neoproterozoic to
222 Paleozoic long-lived accretionary orogeny in the northern Tarim Craton. Tectonics,
223 33(3), 302-329.
224 Guillot, S., Hattori, K., Agard, P., Schwartz, S., & Vidal, O. (2009). Exhumation processes in
225 oceanic and continental subduction contexts: a review. Subduction zone geodynamics,
226 175-205.

Guo, Z. J., Yin, A., Robinson, A., & Jia, C. Z. (2005). Geochronology and geochemistry of deep-drill-core samples from the basement of the central Tarim basin. Journal of Asian Earth Sciences, 25(1), 45-56.

Han, B.-F., He, G.-Q., Wang, X.-C., & Guo, Z.-J. (2011). Late Carboniferous collision between the Tarim and Kazakhstan–Yili terranes in the western segment of the South Tian Shan Orogen, Central Asia, and implications for the Northern Xinjiang, western China. Earth-Science Reviews, 109(3-4), 74-93.

Hawkins, R., & Sambridge, M. (2019). An Adjoint Technique for Estimation of Interstation Phase and Group Dispersion from Ambient Noise Cross Correlations. Bulletin of the Seismological Society of America, 109(5), 1716-1728. https://doi.org/10.1785/0120190060

He, R., Shang, X., Yu, C., Zhang, H., & Van der Hilst, R. D. (2014). A unified map of Moho depth and Vp/Vs ratio of continental China by receiver function analysis. Geophysical Journal International, 199(3), 1910-1918.

Jia, C. (1997). Tectonic characteristics and petroleum, Tarim basin, China. Petroleum Industry Press.

Koulakov, I. (2011). High-frequency P and S velocity anomalies in the upper mantle beneath Asia from inversion of worldwide traveltime data. Journal of Geophysical Research, 116(B4).

Kufner, S. K., Schurr, B., Sippl, C., Yuan, X., Ratschbacher, L., Ischuk, A., ... & Tilmann, F. (2016). Deep India meets deep Asia: Lithospheric indentation, delamination and break-off under Pamir and Hindu Kush (Central Asia). Earth and Planetary Science Letters, 435, 171-184.

Li, W., Chen, Y., Yuan, X., Xiao W, Windley, B. F. (2022) Intracontinental deformation of the Tianshan Orogen in response to India-Asia collision. Nature Communications 13, 3738.

Malusà, M. G., Guillot, S., Zhao, L., Paul, A., Solarino, S., Dumont, T., ... & Yuan, H. (2021). The Deep Structure of the Alps Based on the CIFALPS Seismic Experiment: A Synthesis. Geochemistry, Geophysics, Geosystems, 22(3), e2020GC009466.

McKenzie, D. P. (1969). Speculations on the consequences and causes of plate motions. Geophysical Journal International, 18(1), 1-32.

Molnar, P., & Tapponnier, P. (1975). Cenozoic tectonics of Asia: effects of a continental collision. Science, 189(4201), 419-426.

Sang, M., Xiao, W., Bakirov, A., Orozbaev, R., Sakiev, K., & Zhou, K. (2016). Oblique wedge extrusion of UHP/HP complexes in the Late Triassic: structural analysis and zircon ages of the Atbashi Complex, South Tianshan, Kyrgyzstan. International Geology Review, 59(10), 1369-1389.

Shu, L., Wang, B., Yang, F., Lu, H., Charvet, J., and Laurent-Charvet, S., 2003, Polyphase tectonic events and Mesozoic-Cenozoic basin-range coupling in the Chinese Tianshan belt: Acta Geologica Sinica, 77(4), 457-467.

Sun, W., Zhao, L., Malusà, M. G., Guillot, S., & Fu, L. Y. (2019). 3-D Pn tomography reveals continental subduction at the boundaries of the Adriatic microplate in the absence of a precursor oceanic slab. Earth and Planetary Science Letters, 510, 131-141.

Sun, W., Zhao, L., Yuan, H., and Fu, L. Y., 2020, Sharpness of the Midlithospheric Discontinuities and Craton Evolution in North China: Journal of Geophysical Research: Solid Earth, 125(9). DOI: 10.1029/2019jb018594.

Wang, B., Zhai, Y., Kapp, P., de Jong, K., Zhong, L., Liu, H., et al. (2017). Accretionary tectonics of back-arc oceanic basins in the South Tianshan: Insights from structural, geochronological, and geochemical studies of the Wuwamen ophiolite mélange. GSA Bulletin, 130(1-2), 284-306. https://doi.org/10.1130/B31397.1

Wang, M., Zhang, J., Zhang, B., Liu, K., & Ge, M. (2016). Bi-directional subduction of the South Tianshan Ocean during the Late Silurian: Magmatic records from both the southern Central Tianshan Block and northern Tarim Craton. Journal of Asian Earth Sciences, 128, 64-78. https://www.sciencedirect.com/science/article/pii/S1367912016302115

Xiao, W., Windley, B. F., Allen, M. B., & Han, C. (2013). Paleozoic multiple accretionary and collisional tectonics of the Chinese Tianshan orogenic collage. Gondwana Research, 23(4), 1316-1341.

Xiao, W., Windley, B. F., Sun, S., Li, J., Huang, B., Han, C., et al. (2015). A Tale of Amalgamation of Three Permo-Triassic Collage Systems in Central Asia: Oroclines, Sutures, and Terminal Accretion. Annual Review of Earth and Planetary Sciences, 43(1), 477-507.

Xu, Y. G., Wei, X., Luo, Z. Y., Liu, H. Q., & Cao, J. (2014). The Early Permian Tarim Large Igneous Province: main characteristics and a plume incubation model. Lithos, 204, 20-35.

Xu, X., Zuza, A. V., Yin, A., Lin, X., Chen, H., & Yang, S. (2021). Permian plume-strengthened Tarim lithosphere controls the Cenozoic deformation pattern of the Himalayan-Tibetan orogen. Geology, 49(1), 96-100.

294 Yang, H., Wu, G., Kusky, T. M., Chen, Y., & Xiao, Y. (2018). Paleoproterozoic assembly of the
295 North and South Tarim terranes: New insights from deep seismic profiles and
296 Precambrian granite cores. Precambrian Research, 305, 151-165.
297 Yoshizawa, K., & Ekström, G. (2010). Automated multimode phase speed measurements for
298 high-resolution regional-scale tomography: application to North America. Geophysical
299 Journal International, 183(3), 1538-1558.
300 Zubovich, A. V., Wang, X.-q., Scherba, Y. G., Schelochkov, G. G., Reilinger, R., Reigber, C., et
301 al. (2010). GPS velocity field for the Tien Shan and surrounding regions. Tectonics,
302 29(6), TC6014.
303

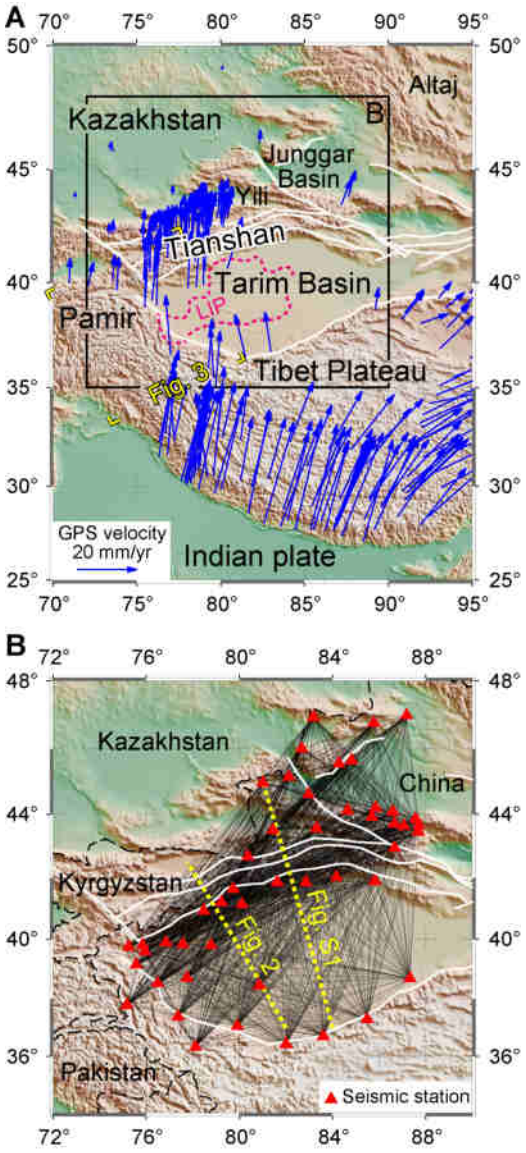

Figure 1. Tectonic setting and experiment set up. A) Shaded relief map of the Tarim basin and surrounding regions showing major tectonic lines (in white), GPS velocity measurements relative to Eurasia (Gan et al., 2007; Zubovich et al., 2010) and the distribution of Permian basalts of the Tarim Large Igneous Province (LIP, dashed magenta line) (Xu et al., 2021). B) Distribution of seismic stations (red triangles) and seismic ray paths of surface waves analyzed in this work (thin black lines). Political boundaries (dashed black lines) and locations of inverted velocity profiles (dashed yellow lines) are also shown.

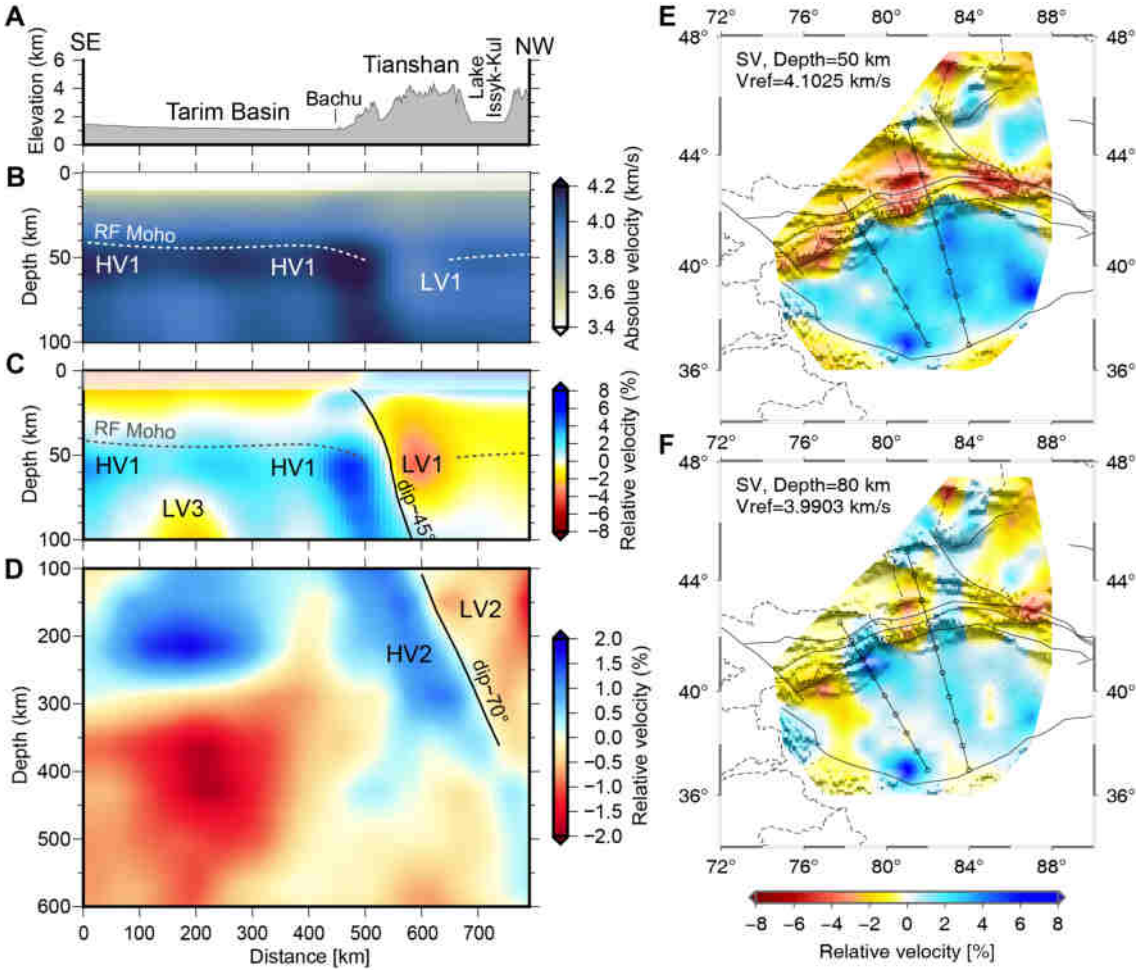

Figure 2. Seismic tomography profile from the southern edge of the Tarim basin to the Issyk-Kul Lake, Kyrgyzstan. A) Topographic profile (see location in Fig. 1A). B) Absolute shear wave velocity structure in the 0-100 km depth range from Rayleigh wave dispersion (this study). The top of the Tarim slab (thick black line) and the Moho from receiver function (dashed grey line, after He et al., 2014) are shown. C) Relative S-wave velocity structure in the 0-100 km depth range (this study). The reference velocity is the average of the 3-D velocity volume in depth. D) P-wave velocity structure in the 100-600 km depth range (after Koulakov, 2011). Please note the vertically exaggerated scale among B)-D). E-F) Depth slices of inverted S-wave velocity at 50 km and 80 km depth. The high-velocity (HV1, 2) and low-velocity (LV1-3) features are discussed in the main text.

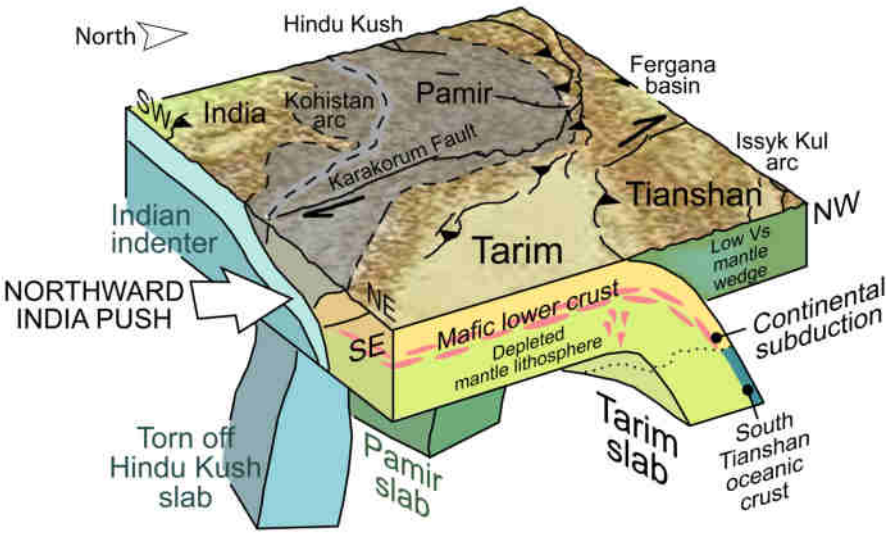

Figure 3. Summary 3-D model of the deep tectonic structure beneath Tarim, Tianshan and Pamir. The SW-NE face of the model is based on Bloch et al. (2021). The south-dipping Pamir slab and the torn off Hindu Kush slab are from Kufner et al. (2016).